

CONVEX microfluidic devices: a new microscale agile manufacturing pipeline for material extrusion additive manufacturing

Amirpasha Moetazedian^{a*}, Vahid Nasrollahi^b, Alessia Candeo^c, Liam Cox^d, Liam M. Grover^e, Gowsihan Poologasundarampillai^{a**}

^aSchool of Dentistry, Institute of Clinical Sciences, University of Birmingham, Edgbaston, B5 7EG, United Kingdom

^bDepartment of Mechanical Engineering, University of Birmingham, Edgbaston B15 2TT, United Kingdom

^cDipartimento di Fisica, Politecnico di Milano, Piazza Leonardo da Vinci 32, 20133 Milano, Italy

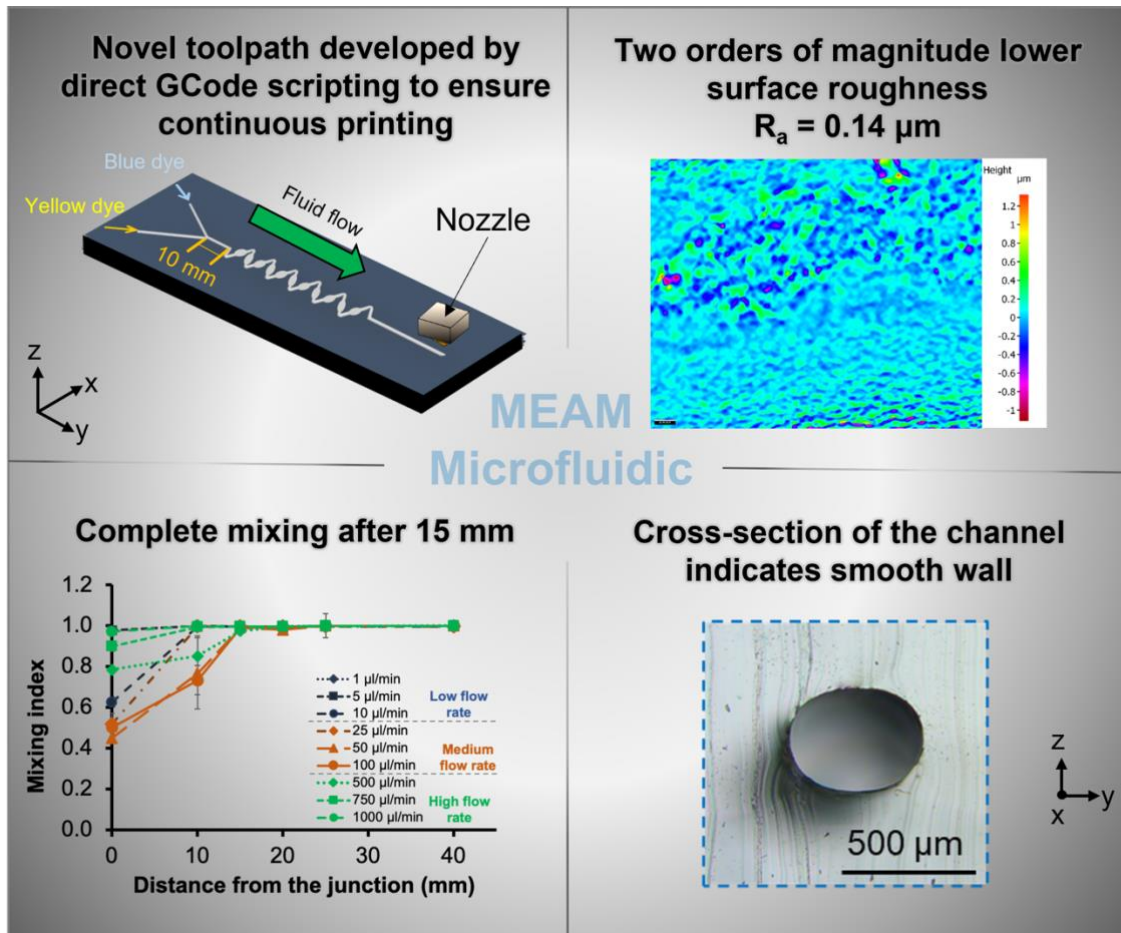
^dSchool of Chemistry, University of Birmingham, Edgbaston, Birmingham, B15 2TT, United Kingdom

^eSchool of Chemical Engineering, University of Birmingham, Edgbaston B15 2TT, United Kingdom

* Corresponding author email address: a.moetazedian@bham.ac.uk

** Corresponding author email address: g.poologasundarampillai@bham.ac.uk

Graphical abstract



Nomenclature

- ABS – acrylonitrile butadiene styrene
- AM – additive manufacturing
- CONVEX – CONTinuously Varied EXtrusion
- DI – deionised water
- EFW – extruded filament width
- FDM – fused deposition modelling
- FFF – fused filament fabrication
- LH – layer height
- LOC – lab-on-a-chip
- MEAM – material extrusion additive manufacturing
- PDMS – polydimethylsiloxane
- PLA – polylactide

R_a – surface roughness
Re – Reynolds number
ROI – region of interest
RT – room temperature
SEM – scanning electron microscopy
SLA – stereolithography
TPU – thermoplastic polyurethane

Abstract

This study is the first to report the fabrication of complex microfluidic devices based on CONTinuously Varied EXtrusion (CONVEX) of extruded filament in material extrusion additive manufacturing (MEAM). A range of complex geometries and channel widths (100–400 μm) were developed by direct GCode scripting including passive mixers of hexagonal, diamond, zigzag and variable-width zigzag (V-zigzag) and hydrodynamic flow focusing components. For each design, a single layer of filament was deposited as the nozzle moved in the X or Y direction, while simultaneously controlling the extrusion volume and printing speed to achieve seamless Y- or cross-junction channels. The novel V-zigzag toolpath design required deposition at varying printing speed along the path, to create the zigzag structure with variable width (200% of nozzle diameter) at pre-determined locations. The passive mixer regions were selectively exposed to acetone for 10 s to reduce the surface roughness of channels before embedding in the polydimethylsiloxane (PDMS). Device structural and fluid flow properties were investigated to generate insights on the impact of manufactured geometry on performance. Microscopic analysis showed the combination of novel manufacturing and chemical treatment reduced the surface roughness of all designs by two orders of magnitude compared to typical values for MEAM parts. Fluid mixing dynamics of microfluidic devices with 400 μm channel widths were measured from 1–1000 $\mu\text{l}\cdot\text{min}^{-1}$. V-zigzag mixers achieved complete mixing rapidly irrespective of flow rates after only 15 mm following two liquids coming into contact along the flow direction. By contrast, the mixing performance progressively decreased for the other designs as the flow rate increased from 50 to 100 $\mu\text{l}\cdot\text{min}^{-1}$, highlighting the important effect of geometry. It was established that the variable-width microscale modification in V-zigzag enhances mixing by promoting directional changes in fluid flow within the channel, affording better mixing performance even at

high flow rates compared to a conventional zigzag design. The resilience and robustness of this manufacturing strategy is demonstrated by pushing the boundaries in AM to produce channels with cross-section of $100 \times 100 \mu\text{m}$ with high repeatability. Case studies demonstrated the applicability of the newly developed microfluidic devices for a wide range of microfluidic applications including fluidic-chip droplet generator and flow focusing printhead capabilities to precisely control the width of multi-material fluid sheaths.

Keywords: Additive manufacturing; Microfluidic; Droplet generator; Mixing index; Multi-material printing

1 Introduction

Fluid manipulation and delivery, in particular spatiotemporal control of fluid composition and flow within milli- and micro-fluidic devices, underpins several advanced setups and technologies employed in regenerative medicine approaches, including three-dimensional (3D) bioprinting, organ-on-a-chip, minimally invasive delivery of cells, molecules and biomaterials and others [1–7]. Reactive mixing of two different fluids in microfluidics presents a challenge due to fluid flow in microfluidic devices is often laminar – characterised by low Reynolds numbers (Re) due to the small channel size and low flow rates – making effective and homogenous mixing of fluids challenging [4,8]. Successful mixing of two fluids can be further hindered by increasing the flow rate [2,9–11]. To address this drawback, two main types of mixing systems, namely passive and active mixers have been introduced to transform laminar into turbulent flow [4]. Passive mixers are fabricated by modifying the configuration and structural geometry of the channels, while active mixers use external energy sources to induce diffusion and chaotic advection mixing [4]. Although both mixer systems enhance the mixing performance of microfluidic devices at low flow rates (i.e., $1\text{--}10 \mu\text{l}\cdot\text{min}^{-1}$) due to diffusion at the boundaries of the fluidic layers, obtaining complete mixing at higher flow rates (i.e., $100\text{--}1000 \mu\text{l}\cdot\text{min}^{-1}$) remains challenging [9,12].

Microfluidic devices are traditionally fabricated from polydimethylsiloxane (PDMS), due to its affordability, biocompatibility for implantable devices and transparency [13].

The process is well established [14,15] and involves a series of multi-step manufacturing processes which makes it difficult to automate, time-consuming, resource-heavy and difficult for wide-spread use [5,14–16]. All of this drives the costs high, with individual chips costing over \$200 [13,17], even before considering cleanroom fees. With increasing emphasis on translation and low-cost microfluidic devices, such fabrication methods are facing a '*manufacturability roadblock*' [18].

Additive manufacturing (AM) platforms offer a compelling solution to overcoming this manufacturing roadblock. AM is transforming research and industrial sectors thanks to its capacity to rapidly and reproducibly fabricate bespoke parts with intricate geometries [19]. In the last two decades, AM technologies have garnered considerable investment from the healthcare sector as they enable the development of patient-specific implants, drug-delivery devices and 3D *in vitro* tissue models [19]. Recent developments in AM technologies and custom toolpaths have generated new opportunities to capitalise on the fabrication of high-value functional parts including microfluidic devices [20,21]. Material extrusion additive manufacturing (MEAM), also referred to as fused deposition modelling (FDM) and fused filament fabrication (FFF) [2,10,21–23], stereolithography (SLA) [24,25] and inkjet technologies [24,26] are commonly used to fabricate microfluidic devices. Of these, MEAM is the most affordable (price per device); with a wide selection of materials and minimal post-processing steps, all factors that make it an ideal choice for assembling low-cost microfluidic devices [27]. MEAM involves the deposition of a molten polymer via a heated nozzle onto a print platform. The deposited filament rapidly solidifies due to the temperature difference between the nozzle and the environment. The desired part is created by moving the nozzle in the X and Y planes, parallel to the print platform, to generate layers of parts sequentially. Lowering the print platform in the Z direction upon completion of each layer enables deposition of subsequent layers, leading to a layer-wise production. The completed part is the physical embodiment of the toolpath and appears as stacked micro-slices [28,29].

Several studies have demonstrated the use of the MEAM technique for fabricating microfluidic devices, either by direct printing from polylactide (PLA) [5,23,30], thermoplastic polyurethane (TPU) [31], and acrylonitrile butadiene styrene (ABS) [2,22], or indirect printing using MEAM parts as a sacrificial template by removing the

features embedded in the matrix of choice [22,32]. Direct printing is the faster method; however, the layer-wise production of devices inherently increases surface roughness. While some studies have utilised this roughness (i.e., ridges) to improve mixing efficiency [2,33,34], for certain applications where cell-laden hydrogels flow into the channels, the presence of ridges can result in particles and fluid stagnating, causing them to be permanently stuck, damaging the cells during the process or trapping them irrecoverably within the channel [5]. In addition, current MEAM microfluidic devices have employed very simple designs for passive mixers e.g. straight Y-channels and serpentine channels [31,32] or are formed by soldering together extruded filaments [22], which compounds effective mixing. As a result, state-of-the-art MEAM microfluidic devices can suffer from low optical transparency, low resolution, difficulties in achieving leak-free structures, poor surface finish ($R_a \approx 10.9 \mu\text{m}$ vs $0.35 \mu\text{m}$ for laser-based AM) and limited capabilities to create complex passive mixers to obtain homogeneous solutions [21,35], which is hampering their application and translation. Bhattacharjee et al. [18] identified two key reasons for the current limitations of MEAM microfluidic fabrication technology: (i) the extruded filament cannot be joined arbitrarily at the intersections; and (ii) it is impossible to achieve seamless structures. These limitations arise from the CAD models slicing the model into thin layers, and generating toolpath per layer to start the printing process [19,20]. We have previously shown that slicer software prevents the full potential of MEAM printers to be realised, since it considers each extruded filament to have a constant aspect ratio, and the part is effectively filled by positioning filaments side-by-side (or according to the chosen infill pattern) [19]. The CONTinuously Varied EXtrusion (CONVEX) method directly addresses these limitations [19]. This design approach enables the production of intricate structures without the defects and voids that are found in comparable structures printed by slicer software [19].

Here, a manufacturing pipeline using the CONVEX approach has been developed to produce seamless ABS sacrificial channels embedded in PDMS coupled with complex passive mixer geometries. This design approach allows the fabrication of microfluidic devices with continuously variable width mixer systems, which are impossible to produce using conventional slicer software. To illustrate the value of directly controlling the printing process rather than the printer itself, we demonstrate reproducible formation of channels, utilising a commercially available MEAM printer (cost \$300), to

fabricate high-quality MEAM microfluidic devices (Section 4.1). We improve by two orders of magnitude the surface roughness of the channels beyond the typical values reported in the literature, using a practical processing technology in which a droplet of acetone is directly applied to the ABS channels for 10 s to remove any residual surface texture created by the nozzle movement (Section 4.2). The mixing properties of the MEAM microfluidic devices were examined from 1–1000 $\mu\text{l}\cdot\text{min}^{-1}$ to showcase the benefits of a new variable-width zigzag mixer over conventional designs (Section 4.3). The transferability of the manufacturing platform to smaller channel sizes suitable for biological and chemical assays is demonstrated by manufacturing Y-channels with a cross-section of 0.1 mm \times 0.1 mm with high reproducibility (Section 4.4). The applicability of the newly developed manufacturing pipeline is discussed (Section 4.5), highlighting new opportunities to design microfluidic printheads for 3D bioprinting of hydrogels and droplet generator chips for use in biological and chemical assays. This manufacturing pipeline will be fundamental for development of new generation of MEAM microfluidic devices with a wide range of applications in microfluidic field.

2 Material and methods

2.1 Materials

White ABS filament (Rasie3D[®] Premium ABS) with 1.75 mm diameter was used to manufacture MEAM channels. Sylgard[®] 184 and its curing agent (Dow Corning) was used as a matrix to embed the ABS channels. Acetone (analytical purity 99.6%) from Fisher Scientific was used for chemical treatment. Tygon tubing kit for microfluidics was supplied by Darwin Microfluidics.

2.2 Additive manufacturing process

A Creality Ender 3 V2 MEAM system with a 0.4 mm nozzle diameter was used to extrude a continuous single layer of ABS filament. Custom GCode commands (series of commands controlling the MEAM printer) were generated using an open-source FullControl GCode designer software [20] with the set printing parameters (Table 1). Y-channels (60 mm long) were printed with the dimensions schematically illustrated in Figure 1. Four passive mixer designs were manufactured and named as follows: zigzag (for constant-width zigzag, Figure 1a), V-zigzag (for variable-width zigzag, Figure 1b), hex (for hexagonal mixer, Figure 1c), and diamond (for diamond mixer, Figure 1d). To ensure seamless structures for the hex and diamond mixers, the toolpath was defined by movement of the nozzle in continuous loops to fill in the

structures. The toolpath for both zigzag and V-zigzag was designed according to $y = A (\sin \lambda x)$ where A (amplitude) = 1.5 mm and λ (wavelength) = 3.3 mm. These values for A and λ showed the best mixing index in a previous study by Khosravi Parsa et al. [36]. Both zigzag and V-zigzag had the same toolpath, with the exception of the printing speed that was intentionally varied for the latter to enable microscale changes along the channel at designed areas as shown in Figure 1b. The sides of the Y-channels were cut using a razor blade to create the inlets for the solution as shown in Figure 1.

To investigate the transferability of the technology to smaller cross-sections for microfluidic devices, a 0.1 mm nozzle diameter was used to manufacture the same designs but with extruded filament width (EFW) and layer height (LH) of 0.1 mm and 0.1 mm, respectively. The printing speed was reduced by half ($100 \text{ mm}\cdot\text{min}^{-1}$) to ensure the nozzle did not block; the remaining printing parameters were kept the same as tabulated in Table 1.

Table 1 Printing parameters used to produce ABS specimens with Creality Ender system.

| Printing parameters | Value |
|--|--------------|
| Extrusion temperature ($^{\circ}\text{C}$) | 240 |
| Print platform temperature ($^{\circ}\text{C}$) | 100 |
| Printing speed ($\text{mm}\cdot\text{min}^{-1}$) | 200 |
| Extruded layer height (mm) | 0.3 |
| Extruded filament width (mm) | 0.4 |

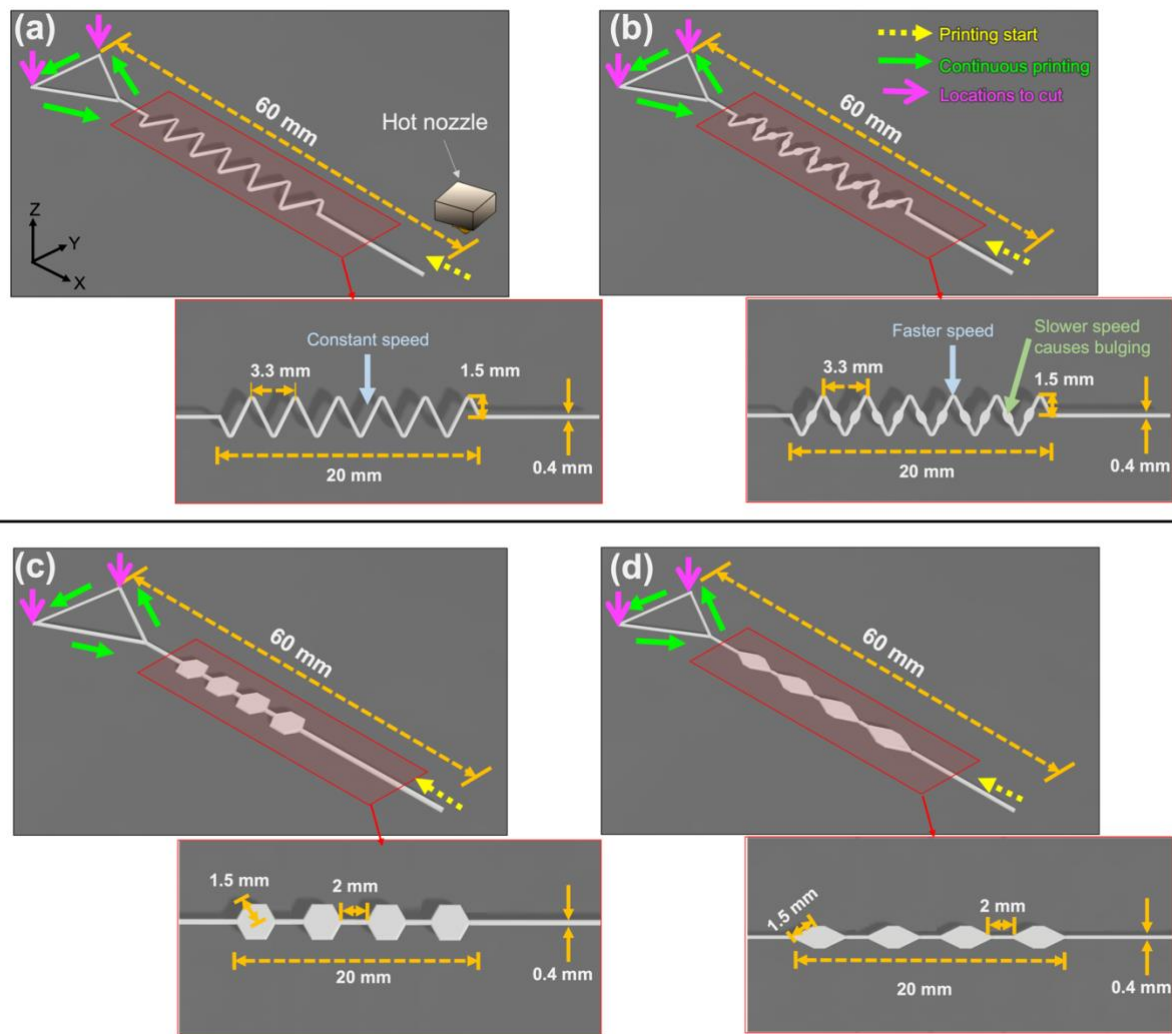


Figure 1 Y-channels with various passive mixer designs were printed using the CONVEX design approach: (a) zigzag, (b) variable-width zigzag (V-zigzag), (c) hex and (d) diamond. Zigzag and V-zigzag designs had the same toolpath, except the printing speed was varied for the V-zigzag to achieve microscale changes in the filament width along the path. The dashed yellow arrow indicates the start of the print, the solid green arrow shows the toolpath for continuous printing of the channels, and the magenta arrow where a razor blade was used to cut the sides of the Y-channels.

2.3 Fabrication of MEAM microfluidic

The manufactured channels (Figure 2a) were selectively exposed to a droplet of acetone (analytical purity 99.6%) using a micropipette at room temperature (RT: 20 °C) for 10 s to remove the surface roughness caused by nozzle movements [Figure 2b (i)]. Preliminary studies (see supporting information, S1) carried out to select the optimum exposure time (from 5 s to 60 s), identified 10 s as the best time to achieve a smooth and stable structure without losing structural integrity [28]. After chemical treatment, the channels were exposed to compressed air at a pressure of 10 psi for 15 min at a

vertical distance of 10 mm from the channels to remove residual acetone [Figure 2b (ii)] under the laboratory conditions (20 °C and 50% relative humidity). Sylgard 184 and its curing agent was prepared at 10:1 ratio according to the manufacturer's recommendations. The PDMS mixture was de-gassed in a vacuum chamber for 30 min to remove bubbles from the solution and then poured into a custom-made mould and cured for 10 min at 70 °C [Figure 2b (iii)]. When the PDMS was semi-cured (i.e., is able to support the ABS channel on the surface), the treated MEAM channel (see Figure 1) was placed on top of the semi-cured PDMS layer and then covered by a new layer of PDMS. The resulting assembly was cured for 2 h at 70 °C until fully set [Figure 2b (iv)]. The cured PDMS was flushed with acetone to dissolve the ABS channels [Figure 2c (i)]. The final MEAM microfluidic had a thickness of 2 mm. To confirm print reliability, the average EFW for 10 channels before and after acetone treatment was measured using a digital calliper. Finally, the mixing index of the different passive mixers was measured.

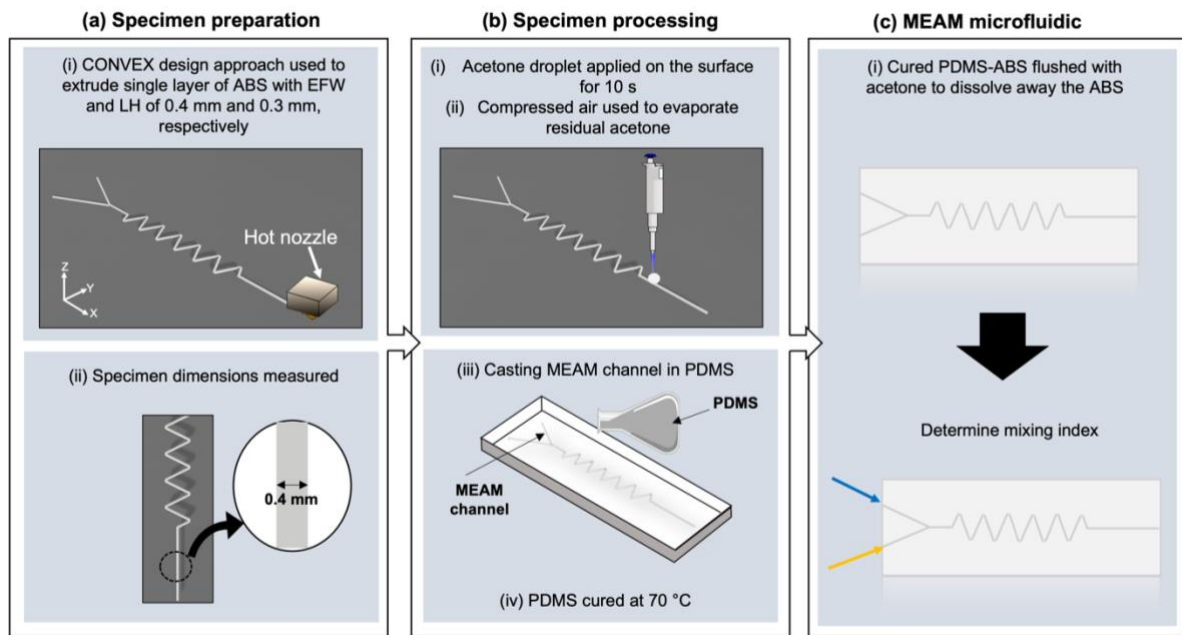


Figure 2 Schematic of the steps involved in fabrication of MEAM microfluidic devices. (a) Specimen preparation: (i) manufacturing of a single layer of Y-channels with various passive mixer designs; (ii) measurement of their EFWs. (b) Specimen processing: (i) reducing the surface roughness of the channels by exposure to acetone for 10 s; (ii) drying before measuring their surface roughness; (iii-iv) channels cast into PDMS to cure at 70 °C for 2 h. (c) Cured PDMS-ABS flushed with acetone to dissolve the ABS polymer. Determination of the mixing index for all four designs by mixing yellow and blue dyes from the two inlets.

2.4 Scanning electron microscopy

A Zeiss EVO MA10 scanning electron microscope (SEM) was used to obtain micrographs of the manufactured channels before and after chemical treatment.

2.5 Surface roughness of channels

An Alicona G5 focus variation microscope (Bruker, Germany) was employed to capture the 3D scans of the Y-channels before and after acetone treatment to quantify surface roughness. In this technique, topographical information is provided by a combination of vertical scanning and focusing of the optical system at different depths (focus-variation technique) [37]. Scans were acquired at specific locations where nozzle movements caused poor surface finish at a 20× magnification. Scans were post-processed using Mountains Premium 7.4 software (Digital surf, France) to create colour-height mapping of the surface. The average surface roughness (R_a) from three replicates was calculated along and perpendicular to the fluid flow.

2.6 Mixing index measurement

The effect of the geometry of the passive mixer on the mixing index of the microfluidic devices was investigated by pumping blue and yellow dyes into the two inlets of the microfluidic device using a dual syringe pump (IPS-14RS, Inovenso) from a 5 mL disposable plastic syringe (Figure 3a). The blue and yellow solutions were prepared by diluting food-grade dye into deionised water (DI) at the ratio of 1:25 according to Mahmud et al. [38]. The viscosity and the density of the solutions was assumed to be similar to DI. The typical flow rates for MEAM microfluidic devices are between 5 and 100 $\mu\text{l}\cdot\text{min}^{-1}$ [5,11,24], so a broad range from 1 to 1000 $\mu\text{l}\cdot\text{min}^{-1}$ was used. The Reynolds number (Re) was quantified according to the method reported by Tsai et al. [9] and varied from 0.047 to 47. Stainless steel needles with 23 gauge were used to connect Tygon tubes (1/16" outer diameter × 0.51 mm inner diameter) to the MEAM microfluidic. A Zeiss Primotech microscope at a 4× magnification was used to capture a series of images at distances of 0, 10, 15, 20, 25 and 40 mm from the junction along the Y-axis (see Figure 3b). To ensure direct comparison across all data, the microscope setting and ambient light were kept constant throughout the experiment.

The mixing index evaluation was based on the RGB values of the pixels in the region of interest (ROI) in the captured micrographs. The ROI was set as a 380 μm × 380 μm square inside the channel. The choice of selecting a smaller square instead of the full

width of 400 μm avoided introducing experimental error by including the shadow on images from the channel walls. For each analysis, three ROIs were used to calculate the mean mixing index. The images were post-processed (Figure 3b) to quantify the mixing index using a Python script (see supporting information, S2) adapted from the MATLAB code by Mahmud et al. [38]. The mixing index was quantified using equation 1 by decoding the respective RGB values for each pixel of the mixed and unmixed solutions.

$$\text{Mixing index} = \frac{N_{\text{mixed}}}{N_{\text{mixed}} + N_{\text{unmixed}}} \quad (1)$$

Where N_{mixed} and N_{unmixed} are the number of pixels classified as mixed and unmixed, respectively, using the following equations:

$$N_{\text{mixed}} = n \left(\{r_{g,\text{min}} \leq R \leq r_{g,\text{max}} \cap g_{g,\text{min}} \leq G \leq g_{g,\text{max}} \cap b_{g,\text{min}} \leq B \leq b_{g,\text{max}}\} \right) \quad (2)$$

and

$$\begin{aligned} N_{\text{unmixed}} &= n \left(\{r_{b,\text{min}} \leq R \leq r_{b,\text{max}} \cap g_{b,\text{min}} \leq G \leq g_{b,\text{max}} \cap b_{b,\text{min}} \leq B \leq b_{b,\text{max}}\} \right) \\ &= n \left(\{r_{y,\text{min}} \leq R \leq r_{y,\text{max}} \cap g_{y,\text{min}} \leq G \leq g_{y,\text{max}} \cap b_{y,\text{min}} \leq B \leq b_{y,\text{max}}\} \right), \quad (3) \end{aligned}$$

The mixing index ranged from 0.0 to 1.0, representing the worst and the best mixing performance, respectively.

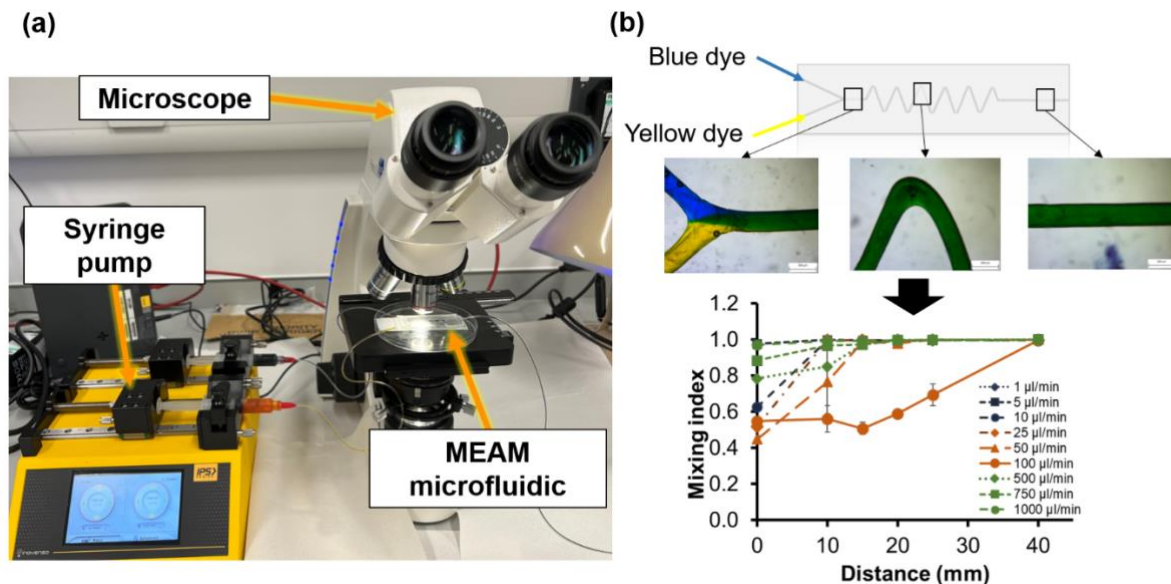


Figure 3 (a) Experimental setup to measure the mixing index for MEAM microfluidic devices. (b) Images captured at various distances used to quantify the mixing index using the Python script developed by the author.

2.7 Case studies

Two case studies were used to demonstrate the use of the new microfluidic fabrication method for regenerative medicine approaches. The same printing parameter settings (see Table 1) were used for both case studies. Cross-junction (3 inlets and 1 outlet) ABS channels were designed to create a device with flow-focusing capabilities. The toolpath was generated using the 'FullControl GCode designer' software to ensure seamless and continuous printing of the filament. The fabricated microfluidic devices (see Section 2.3) were used for two applications: (i) multi-material extrusion, and (ii) droplet generator. For the first application, 2 wt% sodium alginate solution was prepared to demonstrate multi-material extrusion of hydrogels. The flow rate of the shell fluid was varied from 100 to 200 and 500 $\mu\text{l}\cdot\text{min}^{-1}$, while keeping the flow rate of the core fluid at 50 $\mu\text{l}\cdot\text{min}^{-1}$ to examine the effect of ratio of flow rate on the width of the extruded hydrogel. For the second application, mineral oil and DI were used to generate droplets. DI was pumped inside the core channel at a flow rate of 5 $\mu\text{l}\cdot\text{min}^{-1}$ and mineral oil was pumped from the side channels at a flow rate of 10 $\mu\text{l}\cdot\text{min}^{-1}$. The Zeiss Primotech microscope was used to capture images at 4x magnification.

3 Statistical analysis

The data obtained were expressed as means \pm standard deviation. The statistical analyses were performed using Analysis ToolPak in Excel (2016) including one-way analysis of variance (ANOVA) and subsequent *t*-test at significant levels of $p < 0.05$.

4 Results & discussion

The results and discussion are categorised in the following sections:

- 4.1 – Geometrical characterisation of MEAM channels to investigate the print reproducibility.
- 4.2 – Surface roughness characterisation of the channels before and after acetone treatment to measure the improvement in the surface finish.
- 4.3 – Measurement of the mixing properties of various passive mixer design to understand the effect of geometry on the fluidic behaviour.
- 4.4 – Investigation of transferability and resilience of the results using a smaller channel cross-section.

- 4.5 – Discussion of the applications of the findings. Case studies utilise the new understanding developed in Sections 4.1-4 to design and evaluate application of the technology to a MEAM microfluidic printhead and droplet generator chip.

4.1 Geometrical characterisation of channels

Given the important role of AM in translation of low-cost microfluidic devices for biomedical applications, it was deemed important to demonstrate that the manufacturing pipeline developed in this study can produce channels rapidly and with high reproducibility. This section therefore focuses on the geometry of the channels and changes in their dimensions before and after acetone treatment. For the current state-of-the-art MEAM microfluidic devices, considerable variation by up to 25% in dimensions between the CAD and the MEAM part is consistently reported [2,5,11]. This variation occurs since the control over the printing process is limited when using the slicer software, causing under- and/or over-extrusion [39,40]. In the current study, the extrusion volume – that is the amount of material to be deposited – and the printing speed could be precisely controlled and optimised to guarantee the set width (0.4 mm) was achieved. The overall width of the extruded filament was measured using a digital calliper and compared against the set width of 0.4 mm in GCode. As summarised in Figure 4, the mean EFWs for the hex, diamond, zigzag and V-zigzag channels were 0.43 ± 0.01 mm, 0.41 ± 0.02 mm, 0.43 ± 0.01 mm, and 0.41 ± 0.01 mm, respectively. The consistency of these MEAM channels (< 8% difference between EFWs and the set width) is significantly better than previous studies [2,5,11] where up to 0.1 mm variation (25% difference) between the CAD design and the experimentally determined printed part was attained, thus confirming the benefits of direct controlling of the printing process. A significant advance in fabrication of microfluidic devices by MEAM was demonstrated using the CONVEX design approach for generating previously improbable structures, including channels with variable width along the path – V-zigzag (Figure 1b). For the V-zigzag mixer, by directly controlling the printing process, it was possible to create specific regions on the zigzag channels that were 2× wider than the rest of the channel by slowing down the printing speed at these regions. This variation in printing speed cannot be achieved by using slicer software but is readily achieved by direct GCode scripting.

Following acetone treatment, the mean EFW for hex, diamond, zigzag and V-zigzag designs were 0.43 ± 0.01 mm, 0.42 ± 0.01 mm, 0.42 ± 0.01 mm, and 0.42 ± 0.01 mm, respectively; this reveals less than 5% difference between untreated and treated channels. These results confirm that the chemical treatment did not affect the overall dimensions of the channels and highlight how selective acetone treatment can reduce the surface roughness of MEAM channels without affecting other parameters.

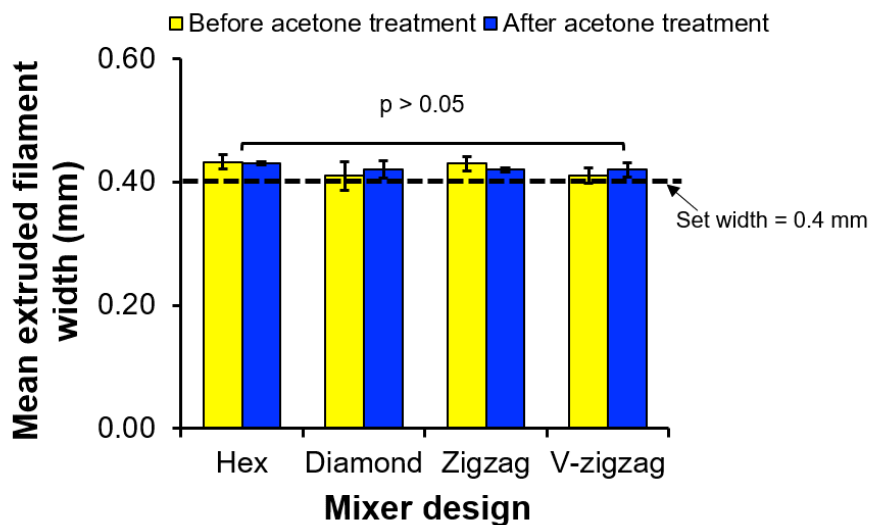


Figure 4 Mean extruded filament width for four MEAM channels before and after acetone treatment. Acetone treatment for 10 s has no significant effect ($p > 0.05$) on the channel dimensions for all designs. Mean values calculated from 10 replicates.

4.2 Effect of acetone on surface roughness of channels

The SEM micrographs of channels before and after acetone treatment along with surface roughness scans are presented in Figure 5. The micrographs of the channels prior to acetone treatment (Figure 5a) show the effect of nozzle movements on the surface texture of the channels, in particular on hex and diamond designs which had higher roughness (max. and min. heights were $+10 \mu\text{m}$ and $-10 \mu\text{m}$, respectively) compared to the zigzag and V-zigzag (max. and min. heights were $+6 \mu\text{m}$ and $-8 \mu\text{m}$, respectively). This is understandable since for both hex and diamond mixers, the toolpath was designed to move the nozzle in a loop at passive mixer locations in order to fill in the space for the hexagonal and diamond mixers (see supporting information, S3 for comparison between slicer and CONVEX). By contrast, the relatively smoother surfaces shown in the micrographs of the zigzag and V-zigzag designs are consistent

with a continuous and unidirectional steady-state movement of the nozzle (i.e., along the print platform).

Acetone treatment had a noticeable effect on the topography of all four channel designs: all four showed a flat surface topography similar to that of injection-moulding parts [41] with no visible texture at the surface. This was confirmed by the colour-map scans; thus, all designs showed a maximum height of 2.4 μm .

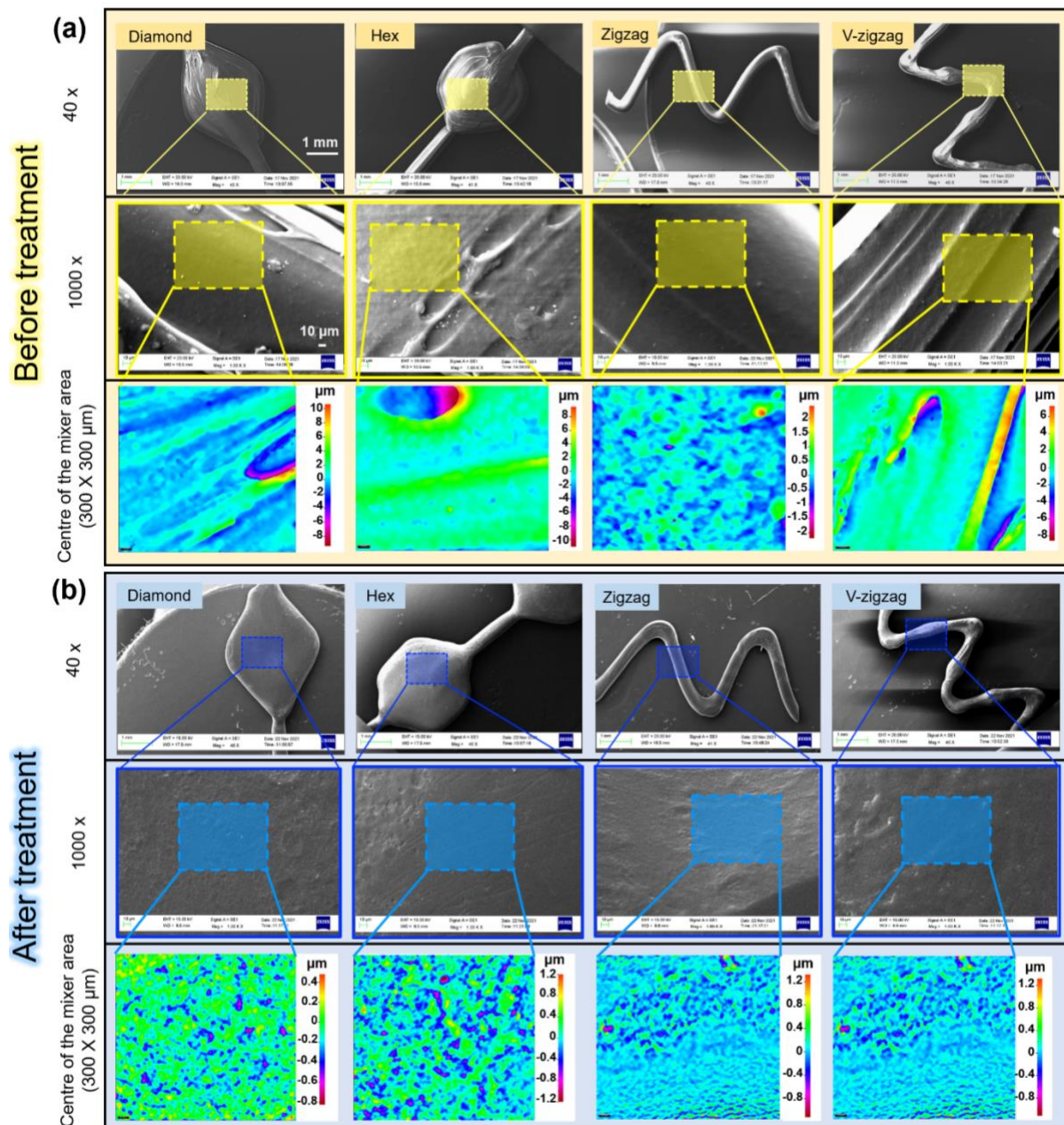


Figure 5 SEM micrographs for mixer designs at two magnifications along with the 2D colour-mapping of the surface, (a) before acetone treatment, and (b) after acetone treatment. Acetone treatment for 10 s considerably improved the surface roughness of all four channel designs.

The surface roughness (R_a) of the MEAM channels was further quantified in two directions, namely along the fluid flow and perpendicular to direction of the fluid flow to investigate the effect of direction on these measurements before and after acetone treatment. Before acetone treatment, the hex and diamond designs had surface roughness values of $0.49 \pm 0.11 \mu\text{m}$ and $0.92 \pm 0.21 \mu\text{m}$, respectively. These values were more than three times higher than values measured for the zigzag ($0.15 \pm 0.01 \mu\text{m}$) and V-zigzag ($0.16 \pm 0.02 \mu\text{m}$) designs. The results supported the SEM micrographs (Figure 5) and evidence the significant effect of nozzle movement on the top surface of the extruded filament. Furthermore, for the hex and diamond designs, the surface roughness was dependent on the direction of measurement. When measured normal to the fluid flow (Figure 6b), values increased by 24.4% and 60.6% for hex and diamond, respectively, compared to the values measured along the fluid flow (Figure 6a). These differences can be understood: for the diamond design, more filaments (4 lines) were needed to fill in the space compared to the Hex design (3 lines). Nevertheless, the hex mixer with the highest surface roughness value still showed over 85% lower surface roughness compared to those reported previously [24]. Such differences arise from the fact that in this study, a single layer of filament is deposited compared with the multi-layer channels in the literature.

The effect of acetone on the surface roughness was investigated by performing measurements of surface roughness along the direction of the fluid flow. The mean surface roughness for the hex, diamond, zigzag and V-zigzag designs were $0.16 \pm 0.07 \mu\text{m}$, $0.17 \pm 0.05 \mu\text{m}$, $0.13 \pm 0.04 \mu\text{m}$, $0.14 \pm 0.02 \mu\text{m}$, respectively, with no considerable variation ($p > 0.05$) between them. Similar values were obtained when surface roughness was measured perpendicular to the fluid flow for the hex and diamond designs ($0.15 \pm 0.05 \mu\text{m}$ and $0.17 \pm 0.03 \mu\text{m}$, respectively), with only 6.4% difference between the two directions. These results demonstrate how acetone treatment reduces surface roughness of the MEAM channels by removing the texture in both directions, creating a flat featureless surface topography, comparable to those produced by injection moulding [41]. The calculated surface roughness in this study was impressively lower (up to 98.7% reduction) than the values reported in the literature for similar MEAM specimens [11].

These findings are significant since one of the main current limitations of MEAM for fabrication of microfluidic devices is poor surface finish, which has been reported to limit the optical performance of structures [11] and lead to cell sedimentation that can obstruct the channels [42]. We have addressed this issue by combining the manufacturing strategy (i.e., printing single layer) with an operationally practical acetone treatment.

The finished MEAM microfluidic devices were visibly transparent due to the use of PDMS as the matrix (Figure 6c). Optical transparency is important for certain applications where high-resolution imaging of the channels, including light-sheet microscopy [43], is necessary to track fluid flow through the channels. A series of images captured at the tip of the nozzle (Figure 6c) were used to examine the smoothness of the channels. All images reveal smooth walls with no indication of ridges or texture, supporting the surface roughness data (Figure 6a-b). Acetone-treated channels were therefore used for the rest of the study to examine the mixing performance of the microfluidic devices.

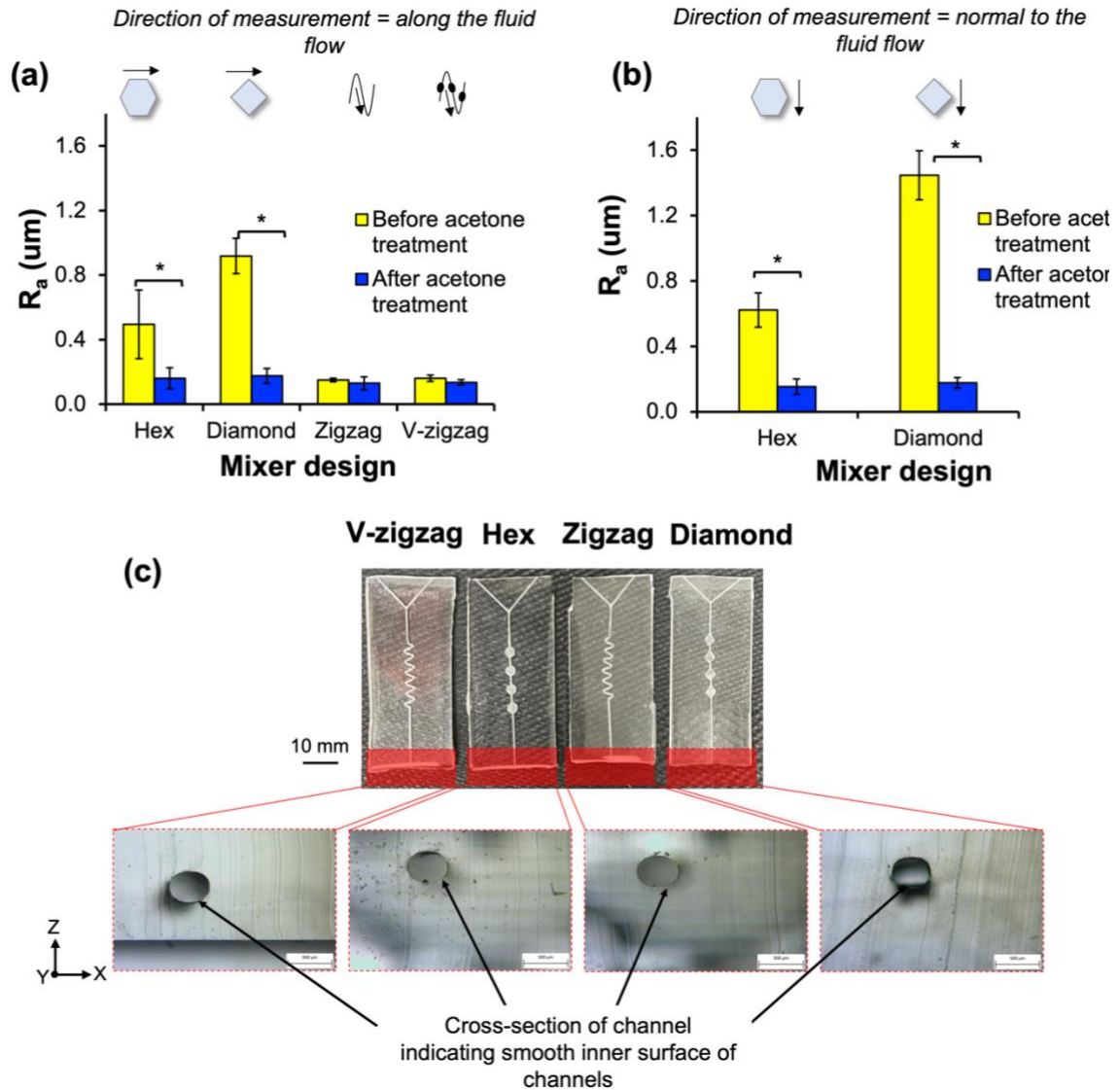


Figure 6 Mean surface roughness (R_a) values measured for all four designs (a) along and (b) normal to the fluid flow. (c) Images after ABS dissolution, revealing smooth channel walls, similar to those produced by lithography. The MEAM microfluidic after dissolving the ABS channels with acetone significantly ($* p < 0.05$) improved the surface roughness for the hex and diamond designs in both directions. For the zigzag and V-zigzag designs, the surface roughness improved but not significantly ($p > 0.05$). Mean values calculated from 3 replicates.

4.3 Effect of passive mixer geometry on fluid mixing quantified with mixing index at different flow rate regimes

4.3.1 Mixing at different locations along the channel for V-zigzag

At all three flow rate regimes: low ($5 \mu\text{l}\cdot\text{min}^{-1}$), medium ($500 \mu\text{l}\cdot\text{min}^{-1}$) and high ($500 \mu\text{l}\cdot\text{min}^{-1}$), complete mixing was achieved after 15 mm, while at $5 \mu\text{l}\cdot\text{min}^{-1}$, complete mixing was observed after 10 mm (Figure 7). The V-zigzag design outperformed in mixing efficiency the current state-of-the-art MEAM microfluidic devices reported in the literature [2,4,10]. This is also true at high flow rates ($100\text{--}1000 \mu\text{l}\cdot\text{min}^{-1}$) where mixing

has proven challenging for other MEAM systems (15 mm vs 24–197 mm in other studies). High mixing performance was only feasible as a result of the CONVEX design approach being coupled with the novel zigzag passive mixer with a continuous variable-width channel to disturb the fluid flow and changes the direction of flow and supported by previous numerical studies of zigzag mixer at Re of 10-200 [44,45]. We postulate that the synergistic effect of the zigzag design and variable width appear to promote a change in direction of fluids, facilitating mixing and allowing complete mixing after only 15 mm.

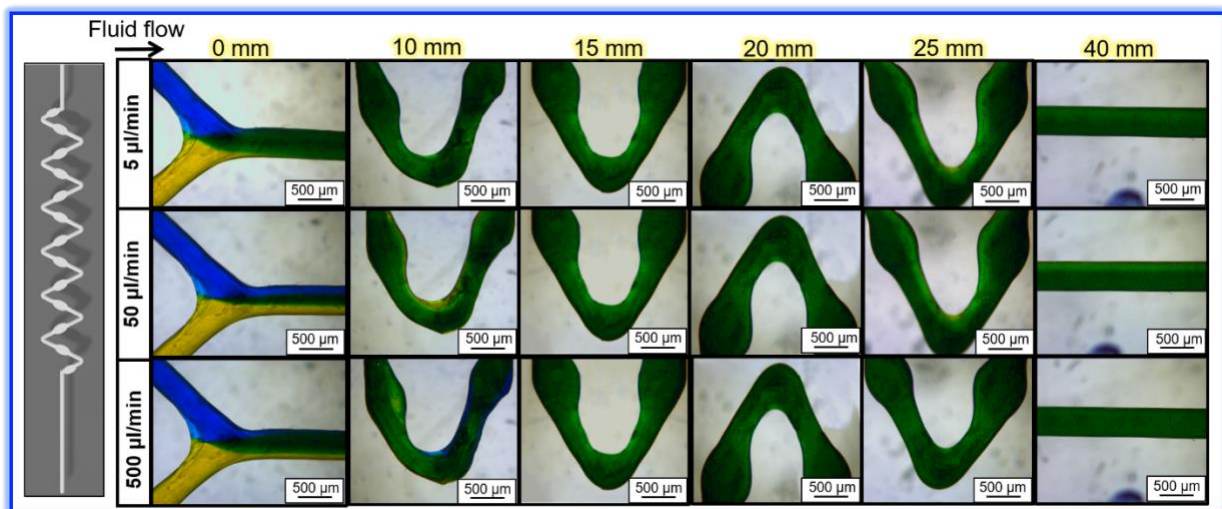


Figure 7 Microscopy images of the V-zigzag channel visualised with blue and yellow fluids progressed along the channels at flow rates of 5, 50 and 500 $\mu\text{l}\cdot\text{min}^{-1}$. At all three flow rate regimes, complete mixing was still achieved after 15 mm along the Y-axis.

4.3.2 Effect of geometry on the mixing index at different flow rates

Based on the results summarised in Figure 7, the mixing index for all four designs was expressed as a function of distance at flow rates of 1, 5, 10, 25, 50, 100, 500, 750 and 1000 $\mu\text{l}\cdot\text{min}^{-1}$ (Figure 8). The obtained results, summarised in Figure 8, are discussed in the following paragraphs.

- **Low flow rate regime (1, 5, 10 $\mu\text{l}\cdot\text{min}^{-1}$)**

At low flow rates no clear difference was found between the mixing results of the four passive mixer designs, demonstrating that the geometry is not critical at this flow rate regime. On the contrary, the effect of varying the flow rate appeared to be important; the 35% decrease in the mixing index at the junction for an order of magnitude increase in flow rate could result in a worse mixing performance initially, but as the fluids progress along the channels, complete mixing is still achieved after 10 mm from the junction. The findings are in good agreement with a previous study by Tsai et al.

[9], who reported similar mixing indices for zigzag channels at flow rates of 1–10 $\mu\text{l}\cdot\text{min}^{-1}$. The trends observed at these low flow rates are reasonable considering Re numbers are in the range 0.047 to 0.47. At such a low Re number, laminar flow dominates and the mixing of two fluids is controlled by Fick's first law of diffusion [9]. According to this law, the mixing performance of two fluids at low flow rate solely relies on the time of diffusion and is driven by the concentration gradient. Therefore, for a given channel length, a lower flow rate provides a longer time for diffusion, and hence better mixing, which explains the decrease in the mixing index at the junction for 10 $\mu\text{l}\cdot\text{min}^{-1}$ compared to the 1 $\mu\text{l}\cdot\text{min}^{-1}$ flow rate.

- **Medium flow rate regime (25, 50, 100 $\mu\text{l}\cdot\text{min}^{-1}$)**

At medium flow rates (Figure 8d-f), which are an order of magnitude faster than those in low flow rate regime (Figure 8a-c), the mixing results were dependent on the geometry of the passive mixers. For example, at a flow rate of 25 $\mu\text{l}\cdot\text{min}^{-1}$, all four designs achieved complete mixing (i.e., mixing index = 1.0) after 10 mm. With an increase in flow rate, the length required to achieve complete mixing also increased, supporting the previous study by Zeraatkar et al. [10]. At a flow rate of 50 $\mu\text{l}\cdot\text{min}^{-1}$, complete mixing was only achieved for the zigzag and V-zigzag designs after 15 mm; the hex and diamond designs had mixing index values of 0.93 ± 0.02 and 0.88 ± 0.06 , respectively, at this distance, highlighting the significant effect of geometry on the mixing.

The dependency of the mixing performance on the geometry of the passive mixer was even more pronounced when the flow rate was increased to 100 $\mu\text{l}\cdot\text{min}^{-1}$. At this flow rate, the best and worst mixer designs were V-zigzag and diamond, respectively. For the V-zigzag design, complete mixing was once again achieved after 15 mm, whereas for the diamond design, the mixing index was 0.90 ± 0.02 after 40 mm. Furthermore, at a distance of 15 mm, the conventional zigzag design had a mixing index value of 0.51 ± 0.03 , 50% lower than the V-zigzag design, which could be explained by the difference in their geometries. The comparison between zigzag and V-zigzag designs supports our hypothesis that the additional microscale changes in the filament width for the newly developed V-zigzag channel may promote a directional change in the fluid flow, effecting a better mixing performance. These results suggest that at a medium flow rate, mixing is not entirely diffusion-based and advective flux starts to become dominant with increasing flow rate, while diffusive flux remains almost constant as it relies only on the diffusion coefficient and concentration gradient [9]. The

results presented in Figure 8 support the earlier study by Tsai et al. [9] who also reported that the zigzag angles fabricated by lithography significantly change the mixing results at flow rates of 40–100 $\mu\text{l}\cdot\text{min}^{-1}$.

- **High flow rate regime (500, 750, 1000 $\mu\text{l}\cdot\text{min}^{-1}$)**

The mixing results for the high flow rate regime are shown in Figure 8 g-i. Under this regime, the novel V-zigzag mixer outperformed the other designs, achieving complete mixing after 15 mm at all flow rates. The diamond design required the longest distance (40 mm) to obtain a combined mean mixing index of 0.98 ± 0.02 at all three flow rates. Increasing the flow rate beyond 500 $\mu\text{l}\cdot\text{min}^{-1}$ improved the mixing results for all designs, possibly due to the formation of microfluidic vortices as previously reported [2,9]. It is commonly reported that the swirling motion of vortices enhances the mixing of two fluids by increasing the contact between them [2,9].

The mixing properties of the MEAM microfluidic device can be summarised as follows:

- 1) With increasing flow rate extent of mixing (mixing index) at a fixed length along the channel decreased.
- 2) This behaviour was identical for all geometries until 100 $\mu\text{l}\cdot\text{min}^{-1}$ was reached.
- 3) At this flow rate, fluids were over 40 mm along the channels before a mixing index of 1 was observed. Whilst for the V-zigzag which outperformed all other designs mixing index of 1 was obtained at 15 mm.
- 4) When the flow rate was further increased the mixing index increased for all the designs to shorter distances.

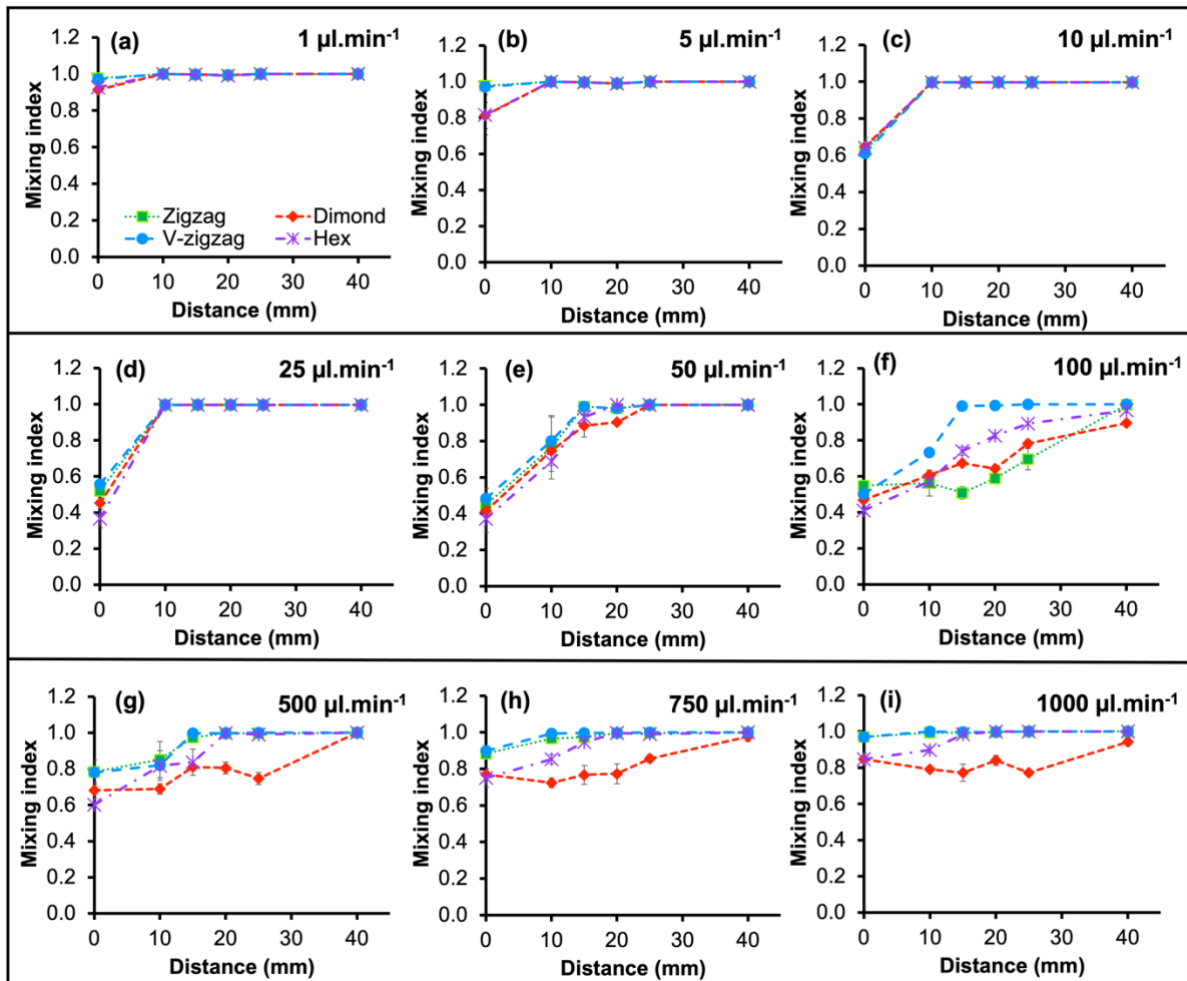


Figure 8 Evolution of mean mixing index for zigzag (square), diamond (diamond), V-zigzag (circle) and hex (cross) designs along the channel at flow rates of (a) 1 $\mu\text{l}\cdot\text{min}^{-1}$, (b) 5 $\mu\text{l}\cdot\text{min}^{-1}$, (c) 10 $\mu\text{l}\cdot\text{min}^{-1}$, (d) 25 $\mu\text{l}\cdot\text{min}^{-1}$, (e) 50 $\mu\text{l}\cdot\text{min}^{-1}$, (f) 100 $\mu\text{l}\cdot\text{min}^{-1}$, (g) 500 $\mu\text{l}\cdot\text{min}^{-1}$, (h) 750 $\mu\text{l}\cdot\text{min}^{-1}$, and (i) and 1000 $\mu\text{l}\cdot\text{min}^{-1}$. The V-zigzag design exhibited the best mixing performance for all flow rates, achieving complete mixing after 15 mm. The diamond and hex designs were more sensitive to the flow rate to achieve > 0.98 mixing.

4.4 Capacity to manufacture MEAM mixers with smaller channel width

Microfluidics with channel width in the range of 0.1-0.01 mm are required for many biomedical applications as it allows reducing the volume of samples, chemical and reagents required to perform the experimental work [46]. To investigate the applicability of this manufacturing platform to this smaller channel size, a 0.1 mm nozzle diameter was used to extrude Y-channels with a cross-section of 0.1 mm × 0.1 mm. The micrographs for V-zigzag channels printed with 0.4 mm and 0.1 mm widths are shown in Figure 10 demonstrating successful printing employing CONVEX design approach. The overall width of the smaller channels was measured by calliper and the mean EFWs of the hex, diamond, zigzag and V-zigzag designs were 0.10 ± 0.01 mm, 0.11 ± 0.02 mm, 0.10 ± 0.01 mm, and 0.10 ± 0.01 mm, respectively, with no significant ($p > 0.05$) variation between these four channel designs (Figure 10c). The closeness of the data (only 9.52% difference) to the set width of 0.1 mm and the small variation between the individual designs, can be attributed to the direct GCode scripting, which allowed optimisation of the printing speed and extrusion rate to ensure the targeted cross-sectional area was achieved. These results demonstrate the advantage of the current methodology compared with previous studies by Felton et al. [5], who investigated the application of MEAM in microfluidic field and showed significant variability in the print success (only 167 successfully printed out of 250 printed channels) for channels with 0.1 mm width.

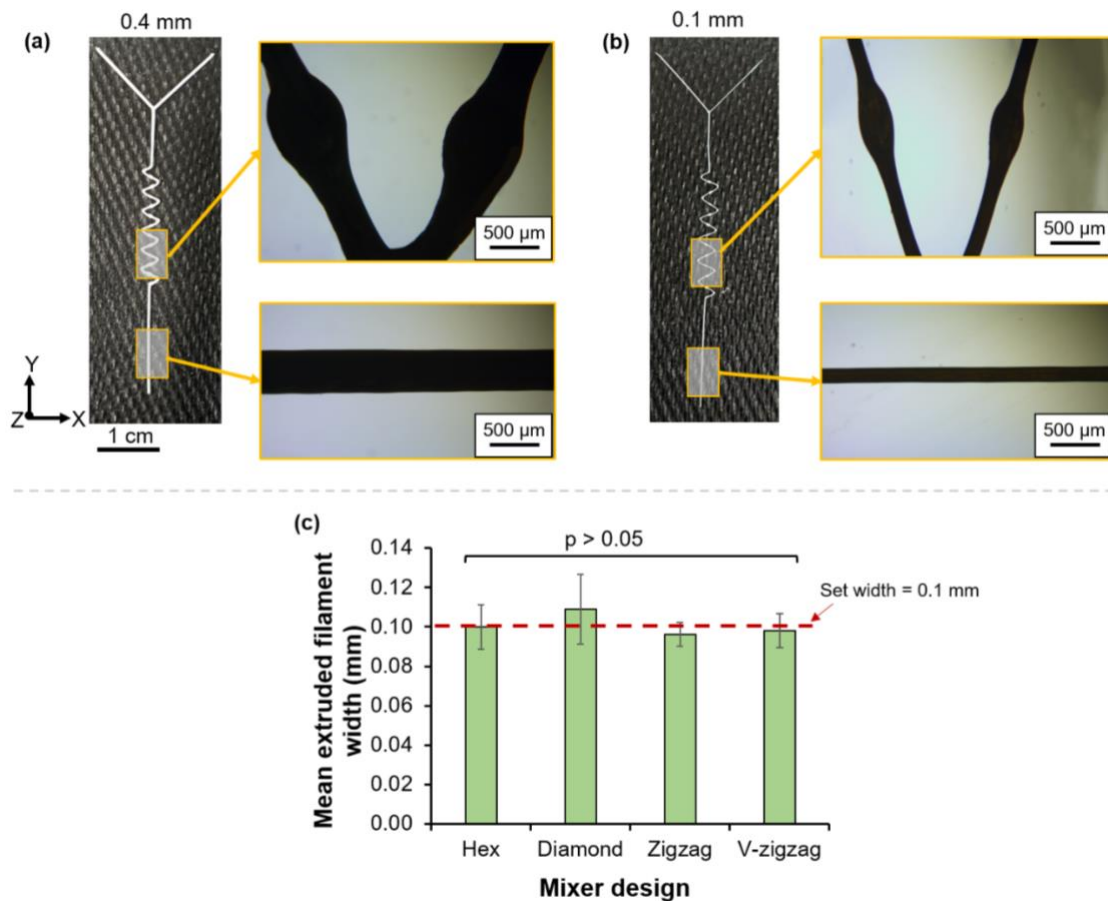


Figure 9 Micrographs of V-zigzag channels printed with EFWs of 0.4 mm (a) and 0.1 mm (b). (c) The mean EFW for passive mixer designs showed high reproducibility in the printing process. Mean values calculated from 10 replicates. See supporting videos for fabrication of all four designs.

4.4.1 Summary

The V-zigzag design showed the best mixing performance, irrespective of flow rates over three orders of magnitude, by maintaining a complete mixing index value (Figure 9). This supports the capacity of V-zigzag design to ensure complete mixing, rapidly even though surface roughness was low. In contrast to the V-zigzag design, for the other designs, three regions are observed. First, in the region with $0.047 < Re < 1.19$, complete mixing is achieved with no significant variation between the designs. Such results suggest that mixing performance is not influenced by the geometry of the mixers and that diffusion is more important in this regime. Beyond that point, mixing performance progressively reduces for the zigzag (by 42.1%), hex (by 18.3%) and diamond (by 36.4%) designs. The transition point was found consistently around $Re = 3$. When the flow rate increased beyond this transition point, the mixing performance for the diamond design continued to worsen (reduced by 18.1%) supporting earlier

studies [11,38,47] that highlight the adverse effect of high flow rates on mixing [11,38,47]. By contrast, other passive mixer designs show a recovery, suggesting a significant effect of channel geometry. The recovery of mixing performance was previously reported by Tsai et al. [9], who also identified a transition point (around $Re = 15$) for zigzag channels fabricated by lithography with a channel width of 0.1 mm. Our results provide strong evidence that the geometry of a passive mixer plays a key role in determining the mixing index for a wide range of flow rates.

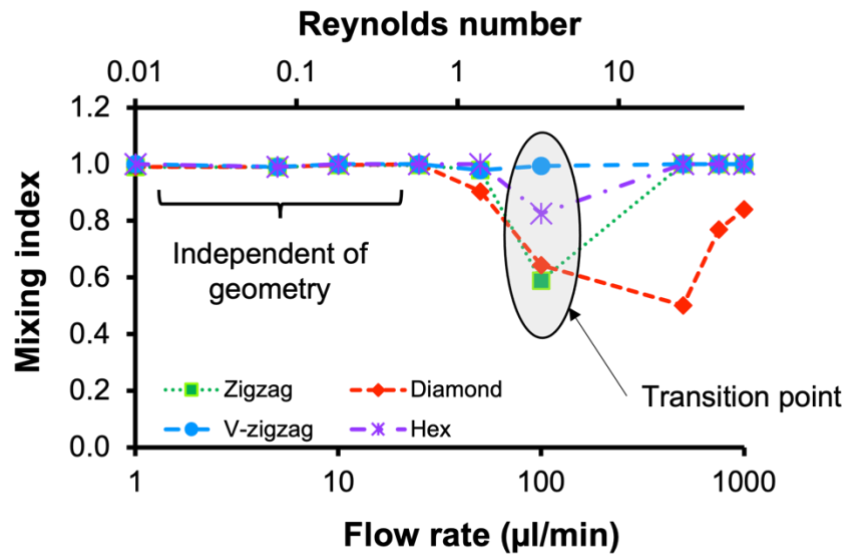


Figure 10 Evolution of mean mixing index for various passive mixer designs vs. flow rate and Reynolds numbers at a distance of 20 mm the junction. The mixing index values for zigzag, diamond and hex were dependent on the Reynolds number where the lowest mixing performance was measured at Re of 3. V-zigzag achieved complete mixing at all flow rates.

A summary of the mixing index, geometrical and physical properties of the V-zigzag microfluidic and existing AM devices in the literature [2,4,10,24] is presented in Table 2. The mixing performance and surface roughness of the V-zigzag is significantly better than currently available AM passive mixer devices (manufactured by MEAM or SLA). Most studies which demonstrated complete mixing only measured the mixing properties at low flow rates ($< 1000 \mu\text{l}\cdot\text{min}^{-1}$) for large channel width (600-900 μm). For conventional lithographic microfluidic devices, fluids behaviour is analysed on a smaller scale (10–100 μm), which makes it easier to control the interactions and movements of samples and reducing the chemical waste. As a result, in this study, it was decided to fabricate MEAM microfluidics with dimensions as close as possible to conventional devices (i.e., 100–400 μm). More importantly, for many microfluidic applications, it is not necessary to use fixed flow rates during the process, thus, the bespoke microfluidic device should operate for a wide range of flow rates. The present

study demonstrated a manufacturing pipeline capable of fabrication of MEAM microfluidic device with a passive mixer to ensure rapid mixing properties even at high flow rates (100–1000 $\mu\text{l}\cdot\text{min}^{-1}$), which previously appeared to be challenging. Therefore, the newly developed microfluidic device can be incorporated into several applications that require high flow rates, including microfluidic filtration.

Table 2 Comparison of key properties of the AM microfluidic devices from the literature and the current study. MEAM – material extrusion additive manufacturing; SLA – stereolithography.

| AM technology | Design of channel | Feature to enhance mixing | Channel dimensions (μm) | Distance to achieve complete mixing (mm) | | | | R_a (μm) | Fully transparent | Ref |
|--------------------|-------------------|-------------------------------|--------------------------------------|--|--|---|--|-------------------------|-------------------|------------|
| | | | | 25 ($\mu\text{l}\cdot\text{min}^{-1}$) | 50 ($\mu\text{l}\cdot\text{min}^{-1}$) | 100 ($\mu\text{l}\cdot\text{min}^{-1}$) | 1000 ($\mu\text{l}\cdot\text{min}^{-1}$) | | | |
| MEAM | Y-channel | Ridges | 900 x 900 | 49 | 69 | ✗ | Not considered | - | ✗ | [10] |
| MEAM | Y-channel | Surface ridges | 750 x 500 | 20 | 20 | 15 | Not considered | 10.97 | ✗ | [24] |
| SLA | Y-channel | - | 750 x 500 | ✗ | ✗ | ✗ | Not considered | 0.44 | ✗ | |
| MEAM | Y-channel | Serpentine | 600 x 600 | 81 | ✗ | ✗ | Not considered | - | ✗ | [4] |
| SLA | Y-channel | Serpentine | 600 x 600 | 151 | ✗ | ✗ | Not considered | - | ✗ | |
| MEAM | Y-channel | Ridges | 750 x 500 | 20 | 20 | ✗ | Not considered | 11.41 | ✗ | [2] |
| SLA | Y-channel | - | 750 x 500 | ✗ | ✗ | ✗ | Not considered | 0.99 | ✗ | |
| *This study (MEAM) | Y-channel | Complex passive mixer designs | 400 x 300 & 100 x 100 | 10 | 15 | 15 | 10 | 0.14 | ✓ | This study |

4.5 Industrial application and case studies

Although previous studies [5,33,48] have demonstrated some promising results for utilising MEAM in the field of microfluidics, there remains significant scope to improve the manufacturing approach to address current limitations in terms of mixing properties, resolution, optical transparency, surface roughness and inclusion of complex passive mixer systems to broaden the microfluidic applications of MEAM. Of AM technologies, SLA and inkjet offer better resolution and surface finish; thus, they are currently preferred to fabricate complex and bespoke microfluidic systems over off-the-shelf microfluidic mixers to precisely control fluids [24]. However, these technologies suffer from expensive post-processing steps, high cost of the printer and consumables (\$3k and \$85k for SLA and inkjet, respectively), and limited selection of materials suitable for biomedical applications [24]. Therefore, currently there is no AM

technology that covers all microfluidics applications, and scientists need to select the best printer technology (i.e., SLA, MEAM or inkjet) depending on the requirements of the device [24]. The current study aimed to address these limitations by proposing a novel manufacturing strategy using a MEAM technology that is a fraction (i.e., \$300) of the cost of SLA and inkjet technologies. By direct GCode scripting, the toolpath was generated based on the CONVEX design approach in a controlled manner; this ensured continuous printing of a single layer filament which eliminated defects and voids and significantly reduced the surface roughness. Incorporating a 10 s acetone treatment into the fabrication pipeline reduced the surface roughness by two orders of magnitude compared to existing MEAM microfluidic devices.

Additional key benefits of the current methodology are the manufacturing cost and time. In this study, a commercially available MEAM printer, costing approximately \$300, was used. The amount of material used per channel was only 13.4 ± 0.2 mg as opposed to ≈ 200 mg needed where the entire device is printed by MEAM [33]. Furthermore, the printing time per channel was approximately 3 min (yields 20 channels in 1 hour), highlighting the rapid production of low-cost MEAM channels of various designs. Although the authors acknowledge that the casting of channels in PDMS takes 2 hours to be completed, the manufacturing approach is nevertheless more affordable and applicable to many biomedical applications than lithography alternatives.

Another advantage of direct GCode scripting is the possibility to create a single manufacturing procedure where the channels are printed and then the acetone is selectively applied to the passive mixer units as a hybrid process. A further crucial advantage of the new manufacturing approach is the adaptability of the strategy. The passive mixer design units are 'modular' and can be repeated numerous times over arbitrary lengths, making them attractive for various applications. This new MEAM manufacturing pipeline is effective and simple and delivered devices with the superior properties (e.g., $R_a = 0.14 \pm 0.02$ μm , fully transparent and complex geometrical features) that are normally found using SLA and inkjet technologies. More importantly, the high surface finish did not adversely influence the mixing performance as has been previously demonstrated for SLA and inkjet devices. Therefore, the MEAM microfluidic device in this study can be employed for a broad range of microfluidic applications

including manipulation of fluidics, organ-on-chips, droplet generator and mixing needed.

4.5.1 Case study 1: Microfluidic printhead for multi-material printing and precise control

Microfluidic printheads offer spatiotemporal control over the printing process, enabling recreation of the structural complexity of native tissues. To date, most commercially available microfluidic printheads are produced using conventional lithography methods. Here, a MEAM microfluidic printhead, capable of controlling the diameter of a deposited filament by flow-focusing (Figure 11b) has been produced. To this end, 2 wt% sodium alginate solution was prepared with and without yellow dye. To examine the level of control over the extrusion width, a range of flow rate ratios between the core and shell fluids from 2, 4 and 10 were investigated. To allow a direct comparison between flow rates, the widths of the core and shell fluids were normalised by the channel width and plotted against different flow rate ratios (Figure 11c). As can be seen in Figure 11b, by only varying the flow rate of the shell fluid, it was possible to consistently control the width of the core and shell fluids. For example, for the ratio of 2:1:2 [Figure 11b(i)], the width for the core fluid was 169.6 μm (57.6% smaller than the channel width). As the flow rate ratio was increased to 4:1:4 [Figure 11b(ii)] and to 10:1:10 [Figure 11b(iii)], core width decreased to 110.3 μm and 39.3 μm , respectively (72.4% and 90.3% smaller than the channel width, respectively). These results show that with flow focusing it is possible to vary the core fluid from 10% to 43% of the channel size (Figure 11c).

4.5.2 Case study 2: Droplet generator for biological and chemical assays

High throughput generation of fluid droplets with fine control on size and shape is vital for various sectors including regenerative medicine and fluid diagnostic. Our MEAM microfluidic with flow-focusing capability was used as a droplet generator chip (Figure 11). The droplet generator chip was demonstrated through formation of water-in-oil microspheres (Figure 11d). Green dye was pumped as the core fluid (aqueous phase) at a flow rate of 5 $\mu\text{l}\cdot\text{min}^{-1}$, and mineral oil at 10 $\mu\text{l}\cdot\text{min}^{-1}$ as the shell fluid. Chips with channel width of 0.4 mm produced uniform droplets of 923 + 28 μm (based on 5 measurements) in a controlled manner as can be seen in Figure 11e. This study demonstrated a specific implementation of the current manufacturing strategy to

produce droplet generator chips. AM technologies have been used to fabricate droplet generators [5,23,24]; however, these devices suffer from limited optical transparency and rough surface finish, which are important for analysing and monitoring the generation and manipulation of droplets [49,50]. The design introduced in this study addresses both of these issues as we can generate a relatively smooth (at 4× magnification) and optically transparent device suitable for automation without any leakage issues. Future studies can easily adapt the current droplet generator chips to examine single-cells analysis, materials synthesis and chemical reactions depending on the specifications and requirements [5,51].

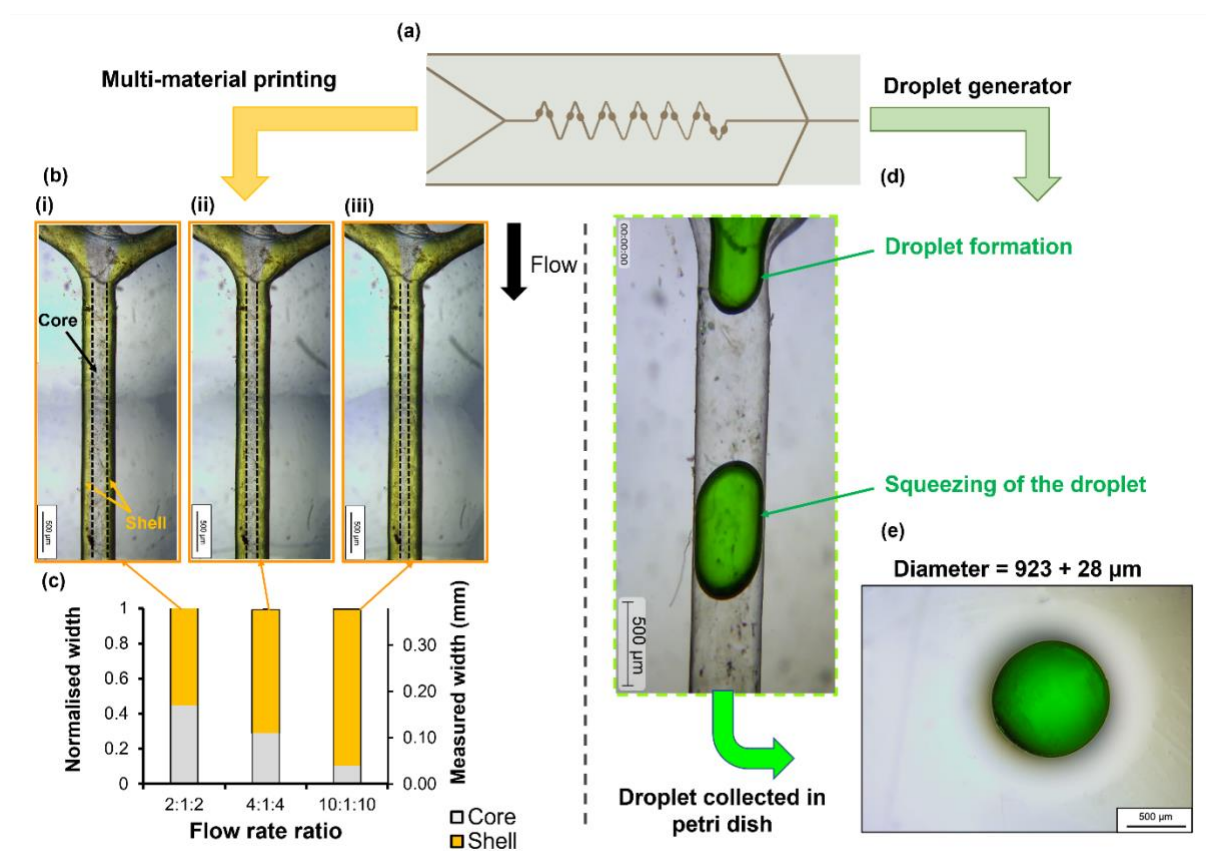


Figure 11 (a) Schematic of a fabricated MEAM microfluidic printhead capable of multi-material extrusion and droplet generation. (b)(i)-(b)(iii) Micrographs of the cross junction showing the changes in width of the core (dashed lines) and shell fluids as the flow rate ratios are varied. (c) Plot of the normalised and actual widths for the core and shell fluids highlighting how the printhead enables highly controllable and dynamic variation of the width of the core fluid. (d) Micrograph of the channel indicating formation of the droplet in the 0.4 mm channel. (e) The deposited spheres formed on a petri dish had a consistent diameter with mean diameter of 923 ± 28 μm from 5 measurements.

5 Conclusions

This study describes the use of a newly developed variable-width zigzag (V-zigzag) passive mixer fabricated by MEAM. The design enabled rapid mixing for a range of flow rates over three orders of magnitude compared to conventional mixer designs (hexagonal, diamond and zigzag). The effect of optimising the toolpath on the surface roughness of microfluidic devices from PDMS was analysed. The results demonstrate that the CONVEX design approach enables simultaneous control of filament deposition while varying extrusion volume and printing speed to achieve seamless structures. Direct application of acetone to the ABS channels for 10 s reduced the surface roughness values by two orders of magnitude compared to typical values for MEAM parts. The influence of passive mixer designs on fluid mixing of the MEAM microfluidic was analysed microscopically. For the V-zigzag design, complete mixing was achieved after 15 mm from the junction irrespective of the flow rate, which we postulate is due to the design promoting directional changes of the fluids and enhancing fluid mixing. For the other designs, mixing performance decreased for medium flow rate regimes by 40-50% depending on the geometry of the mixer. Using a smaller nozzle, it was possible to fabricate channels with cross-section of 0.1 mm × 0.1 mm with high reproducibility and excellent printing quality, opening up new opportunities of MEAM microfluidics in biomedical applications. Two case studies demonstrated two different applications for the newly developed manufacturing strategy. A microfluidic printhead with flow-focusing capabilities enabled precise control over the width of the core fluid from 10% to 43% of the channel width in a controlled manner, demonstrating the potential for multi-material extrusion. A droplet generator chip was also manufactured and tested to demonstrate its suitability for biological-related assays. These new manufacturing capabilities gives confidence in using MEAM for the fabrication of high-quality and complex microfluidic devices.

Acknowledgment

This study was made possible thanks to funding from EPSRC (grant number EP/V051342/1). We would like to thank Harry Felton and Dr Robert Hughes for their constructive feedback.

References

- [1] L. Serex, A. Bertsch, P. Renaud, Microfluidics: A new layer of control for extrusion-based 3D printing, *Micromachines*. 9 (2018).
<https://doi.org/10.3390/mi9020086>.
- [2] F. Li, N.P. Macdonald, R.M. Guijt, M.C. Breadmore, Using Printing Orientation for Tuning Fluidic Behavior in Microfluidic Chips Made by Fused Deposition Modeling 3D Printing, *Anal. Chem.* 89 (2017) 12805–12811.
<https://doi.org/10.1021/acs.analchem.7b03228>.
- [3] C.M.B. Ho, S.H. Ng, K.H.H. Li, Y.J. Yoon, 3D printed microfluidics for biological applications, *Lab Chip*. 15 (2015) 3627–3637.
<https://doi.org/10.1039/c5lc00685f>.
- [4] M. Zeraatkar, D. Filippini, G. Percoco, On the impact of the fabrication method on the performance of 3D printed mixers, *Micromachines*. 10 (2019) 1–10.
<https://doi.org/10.3390/mi10050298>.
- [5] H. Felton, R. Hughes, A. Diaz-Gaxiola, Negligible-cost microfluidic device fabrication using 3D-printed interconnecting channel scaffolds, *PLoS One*. 16 (2021) 1–22. <https://doi.org/10.1371/journal.pone.0245206>.
- [6] C. Dikyol, M. Altunbek, P. Bartolo, B. Koc, Multimaterial bioprinting approaches and their implementations for vascular and vascularized tissues, *Bioprinting*. 24 (2021) e00159. <https://doi.org/10.1016/j.bprint.2021.e00159>.
- [7] D.J. Thomas, Z. Tehrani, B. Redfearn, 3-D printed composite microfluidic pump for wearable biomedical applications, *Addit. Manuf.* 9 (2016) 30–38.
<https://doi.org/10.1016/j.addma.2015.12.004>.
- [8] Z.H. Ward, Kevin and Fan, Mixing in microfluidic devices and enhancement methods, *Top. Rev.* 25 (2015) 1–33. <https://doi.org/10.1088/0960-1317/25/9/094001.Mixing>.
- [9] C.H.D. Tsai, X.Y. Lin, Experimental study on microfluidic mixing with different zigzag angles, *Micromachines*. 10 (2019). <https://doi.org/10.3390/mi10090583>.
- [10] M. Zeraatkar, M.D. de Tullio, A. Pricci, F. Pignatelli, G. Percoco, Exploiting limitations of fused deposition modeling to enhance mixing in 3D printed microfluidic devices, *Rapid Prototyp. J. ahead-of-p* (2021).
<https://doi.org/10.1108/rpj-03-2021-0051>.
- [11] J.C. McDonald, M.L. Chabinyk, S.J. Metallo, J.R. Anderson, A.D. Stroock, G.M. Whitesides, Prototyping of microfluidic devices in poly(dimethylsiloxane)

- using solid-object printing, *Anal. Chem.* 74 (2002) 1537–1545.
<https://doi.org/10.1021/ac010938q>.
- [12] I. Hassan, P.R. Selvaganapathy, A microfluidic printhead with integrated hybrid mixing by sequential injection for multimaterial 3D printing, *Addit. Manuf.* 50 (2022) 102559. <https://doi.org/10.1016/j.addma.2021.102559>.
- [13] A.K. Au, W. Lee, A. Folch, Mail-order microfluidics: Evaluation of stereolithography for the production of microfluidic devices, *Lab Chip.* 14 (2014) 1294–1301. <https://doi.org/10.1039/c3lc51360b>.
- [14] B.K. Gale, A.R. Jafek, C.J. Lambert, B.L. Goenner, H. Moghimifam, U.C. Nze, S.K. Kamarapu, A review of current methods in microfluidic device fabrication and future commercialization prospects, *Inventions.* 3 (2018).
<https://doi.org/10.3390/inventions3030060>.
- [15] P. Kim, K.W. Kwon, M.C. Park, S.H. Lee, S.M. Kim, K.Y. Suh, Soft lithography for microfluidics: A Review, *Biochip J.* 2 (2008) 1–11.
- [16] M.G. Guerra, C. Volpone, L.M. Galantucci, G. Percoco, Photogrammetric measurements of 3D printed microfluidic devices, *Addit. Manuf.* 21 (2018) 53–62. <https://doi.org/10.1016/j.addma.2018.02.013>.
- [17] P. Prabhakar, R.K. Sen, N. Dwivedi, R. Khan, P.R. Solanki, A.K. Srivastava, C. Dhand, 3D-Printed Microfluidics and Potential Biomedical Applications, *Front. Nanotechnol.* 3 (2021) 1–16. <https://doi.org/10.3389/fnano.2021.609355>.
- [18] N. Bhattacharjee, A. Urrios, S. Kang, A. Folch, The upcoming 3D-printing revolution in microfluidics, *Lab Chip.* 16 (2016) 1720–1742.
<https://doi.org/10.1039/c6lc00163g>.
- [19] A. Moetazedian, A.S. Budisuharto, V. V. Silberschmidt, A. Gleadall, CONVEX (CONtinuously Varied EXtrusion): a new scale of design for additive manufacturing, *Addit. Manuf.* 37 (2021) 101576.
<https://doi.org/10.1016/j.addma.2020.101576>.
- [20] A. Gleadall, FullControl GCode Designer: open-source software for unconstrained design in additive manufacturing., *Addit. Manuf.* 46 (2021) 102109.
- [21] R.F. Quero, G. Domingos da Silveira, J.A. Fracassi da Silva, D.P. de Jesus, Understanding and improving FDM 3D printing to fabricate high-resolution and optically transparent microfluidic devices, *Lab Chip.* (2021).
<https://doi.org/10.1039/d1lc00518a>.

- [22] V. Saggiomo, A.H. Velders, Simple 3D Printed Scaffold-Removal Method for the Fabrication of Intricate Microfluidic Devices, *Adv. Sci.* 2 (2015) 1–5. <https://doi.org/10.1002/advs.201500125>.
- [23] S. Tsuda, H. Jaffery, D. Doran, M. Hezwani, P.J. Robbins, M. Yoshida, L. Cronin, Customizable 3D printed “Plug and Play” millifluidic devices for programmable fluidics, *PLoS One.* 10 (2015) 1–13. <https://doi.org/10.1371/journal.pone.0141640>.
- [24] N.P. Macdonald, J.M. Cabot, P. Smejkal, R.M. Guijt, B. Paull, M.C. Breadmore, Comparing Microfluidic Performance of Three-Dimensional (3D) Printing Platforms, *Anal. Chem.* 89 (2017) 3858–3866. <https://doi.org/10.1021/acs.analchem.7b00136>.
- [25] A.I. Shallan, P. Smejkal, M. Corban, R.M. Guijt, M.C. Breadmore, Cost-effective three-dimensional printing of visibly transparent microchips within minutes, *Anal. Chem.* 86 (2014) 3124–3130. <https://doi.org/10.1021/ac4041857>.
- [26] K.G. Lee, K.J. Park, S. Seok, S. Shin, D.H. Kim, J.Y. Park, Y.S. Heo, S.J. Lee, T.J. Lee, 3D printed modules for integrated microfluidic devices, *RSC Adv.* 4 (2014) 32876–32880. <https://doi.org/10.1039/c4ra05072j>.
- [27] R. Su, J. Wen, Q. Su, M.S. Wiederoder, S.J. Koester, J.R. Uzarski, M.C. McAlpine, 3D printed self-supporting elastomeric structures for multifunctional microfluidics, *Sci. Adv.* 6 (2020) 1–10. <https://doi.org/10.1126/sciadv.abc9846>.
- [28] A. Moetazedian, J. Allum, A. Gleadall, E. Mele, V. V Silberschmidt, MaTrEx AM: a new hybrid additive manufacturing process to selectively control mechanical properties, *Addit. Manuf.* 47 (2021) 102337.
- [29] J. Allum, A. Gleadall, V. V. Silberschmidt, ZigZagZ: improving mechanical performance in extrusion additive manufacturing by nonplanar toolpaths, *Addit. Manuf.* 38 (2021). <https://doi.org/https://doi.org/10.1016/j.addma.2020.101715>.
- [30] V. Romanov, R. Samuel, M. Chaharlang, A.R. Jafek, A. Frost, B.K. Gale, FDM 3D Printing of High-Pressure, Heat-Resistant, Transparent Microfluidic Devices, *Anal. Chem.* 90 (2018) 10450–10456. <https://doi.org/10.1021/acs.analchem.8b02356>.
- [31] M.D. Nelson, N. Ramkumar, B.K. Gale, Flexible, transparent, sub-100 μm microfluidic channels with FDM 3D-printed thermoplastic polyurethane, *23rd Int. Conf. Miniaturized Syst. Chem. Life Sci. MicroTAS 2019.* (2019) 1108–

1109.

- [32] W.H. Goh, M. Hashimoto, Dual sacrificial molding: Fabricating 3D microchannels with overhang and helical features, *Micromachines*. 9 (2018) 1–12. <https://doi.org/10.3390/mi9100523>.
- [33] M.A.A. Rehmani, S.A. Jaywant, K.M. Arif, Study of microchannels fabricated using desktop fused deposition modeling systems, *Micromachines*. 12 (2021) 1–20. <https://doi.org/10.3390/mi12010014>.
- [34] F. Kotz, M. Mader, N. Dellen, P. Risch, A. Kick, D. Helmer, B.E. Rapp, Fused deposition modeling of microfluidic chips in polymethylmethacrylate, *Micromachines*. 11 (2020) 5–8. <https://doi.org/10.3390/mi11090873>.
- [35] G.I.J. Salentijn, P.E. Oomen, M. Grajewski, E. Verpoorte, Fused Deposition Modeling 3D Printing for (Bio)analytical Device Fabrication: Procedures, Materials, and Applications, *Anal. Chem.* 89 (2017) 7053–7061. <https://doi.org/10.1021/acs.analchem.7b00828>.
- [36] M. Khosravi Parsa, F. Hormozi, D. Jafari, Mixing enhancement in a passive micromixer with convergent – divergent sinusoidal microchannels and different ratio of amplitude to wave length, *Comput. Fluids*. 105 (2014) 82–90. <https://doi.org/10.1016/j.compfluid.2014.09.024>.
- [37] A. Moetazedian, A. Gleadall, X. Han, V.V. Silberschmidt, Effect of environment on mechanical properties of 3D printed polylactide for biomedical applications, *J. Mech. Behav. Biomed. Mater.* 102 (2020) 103510. <https://doi.org/https://doi.org/10.1016/j.jmbbm.2019.103510>.
- [38] F. Mahmud, K.F. Tamrin, Method for determining mixing index in microfluidics by RGB color model, *Asia-Pacific J. Chem. Eng.* 15 (2020) 1–12. <https://doi.org/10.1002/apj.2407>.
- [39] A. Moetazedian, J. Allum, A. Gleadall, V.V. Silberschmidt, Bulk-material bond strength exists in extrusion additive manufacturing for a wide range of temperatures, speeds and layer times, *3D Print. Addit. Manuf.* (2021).
- [40] V.E. Kuznetsov, A.N. Solonin, A. Tavitov, O. Urzhumtsev, A. Vakulik, Increasing of strength of FFF 3D printed parts by influencing on temperature-related parameters of the process, *Rapid Prototyp. J.* 26 (2020) 107–121. <https://doi.org/10.1108/RPJ-01-2019-0017>.
- [41] G. Tosello, F. Marinello, H.N. Hansen, Characterisation and analysis of microchannels and submicrometre surface roughness of injection moulded

- microfluidic systems using optical metrology, *Plast. Rubber Compos.* 41 (2012) 29–39. <https://doi.org/10.1179/0743289811Y.0000000017>.
- [42] D. Ali, Influence of Cell Transportation Microchannel Wall Quality on Cell Deposition Risk: a DPM Analysis, in: *Int. Conf. Sci. Technol. Eng. Sci. Technol. ICONST EST 2021*, 2021.
- [43] G. Poologasundarampillai, A. Haweet, S.N. Jayash, G. Morgan, J.E. Moore, A. Candeo, Real-time imaging and analysis of cell-hydrogel interplay within an extrusion-bioprinting capillary, *Bioprinting.* 23 (2021) e00144. <https://doi.org/10.1016/j.bprint.2021.e00144>.
- [44] W.A. Fikri Wan Ali, A.A. Hamzah, K. Mustafa, B.Y. Majlis, J. Yunas, Numerical study of zigzag micro mixer with 3d channel dimension, *IEEE Int. Conf. Semicond. Electron. Proceedings, ICSE. 2018-August (2018)* 117–120. <https://doi.org/10.1109/SMELEC.2018.8481300>.
- [45] V. Mengeaud, J. Josserand, H.H. Girault, Mixing processes in a zigzag microchannel: Finite element simulations and optical study, *Anal. Chem.* 74 (2002) 4279–4286. <https://doi.org/10.1021/ac025642e>.
- [46] E.W.K. Young, D.J. Beebe, Fundamentals of microfluidic cell culture in controlled microenvironments, *Chem. Soc. Rev.* 39 (2010) 1036–1048. <https://doi.org/10.1039/b909900j>.
- [47] F. Li, P. Smejkal, N.P. Macdonald, R.M. Guijt, M.C. Breadmore, One-Step Fabrication of a Microfluidic Device with an Integrated Membrane and Embedded Reagents by Multimaterial 3D Printing, *Anal. Chem.* 89 (2017) 4701–4707. <https://doi.org/10.1021/acs.analchem.7b00409>.
- [48] G. Gaal, M. Mendes, T.P. de Almeida, M.H.O. Piazzetta, Â.L. Gobbi, A. Riul, V. Rodrigues, Simplified fabrication of integrated microfluidic devices using fused deposition modeling 3D printing, *Sensors Actuators, B Chem.* 242 (2017) 35–40. <https://doi.org/10.1016/j.snb.2016.10.110>.
- [49] J.M. Zhang, Q. Ji, H. Duan, Three-dimensional printed devices in droplet microfluidics, *Micromachines.* 10 (2019) 1–24. <https://doi.org/10.3390/mi10110754>.
- [50] K. Kowsari, B. Zhang, S. Panjwani, Z. Chen, H. Hingorani, S. Akbari, N.X. Fang, Q. Ge, Photopolymer formulation to minimize feature size, surface roughness, and stair-stepping in digital light processing-based three-dimensional printing, *Addit. Manuf.* 24 (2018) 627–638.

<https://doi.org/10.1016/j.addma.2018.10.037>.

- [51] S. Van Loo, S. Stoukatch, M. Kraft, T. Gilet, Droplet formation by squeezing in a microfluidic cross - junction, *Microfluid. Nanofluidics*. 20 (2016) 1–12.

<https://doi.org/10.1007/s10404-016-1807-1>.